

Search for Supernova Relic Neutrinos at Super-Kamiokande

The Super-Kamiokande Collaboration

M. Malek¹⁷, M. Morii²⁷, S. Fukuda¹, Y. Fukuda¹, M. Ishitsuka¹, Y. Itow¹, T. Kajita¹, J. Kameda¹, K. Kaneyuki¹, K. Kobayashi¹, Y. Koshio¹, M. Miura¹, S. Moriyama¹, M. Nakahata¹, S. Nakayama¹, T. Namba¹, A. Okada¹, T. Ooyabu¹, C. Saji¹, N. Sakurai¹, M. Shiozawa¹, Y. Suzuki¹, H. Takeuchi¹, Y. Takeuchi¹, Y. Totsuka¹, S. Yamada¹, S. Desai², M. Earl², E. Kearns², M.D. Messier^{2,*}, J.L. Stone², L.R. Sulak², C.W. Walter², M. Goldhaber³, T. Barszczak⁴, D. Casper⁴, W. Gajewski⁴, W.R. Kropp⁴, S. Mine⁴, D.W. Liu⁴, M.B. Smy⁴, H.W. Sobel⁴, M.R. Vagins⁴, A. Gago⁵, K.S. Ganezer⁵, W.E. Keig⁵, R.W. Ellsworth⁶, S. Tasaka⁷, A. Kibayashi⁸, J.G. Learned⁸, S. Matsuno⁸, D. Takemori⁸, Y. Hayato⁹, T. Ishii⁹, T. Kobayashi⁹, T. Maruyama^{9,†}, K. Nakamura⁹, Y. Obayashi⁹, Y. Oyama⁹, M. Sakuda⁹, M. Yoshida⁹, M. Kohama^{10,‡}, T. Iwashita¹⁰, A.T. Suzuki¹⁰, A. Ichikawa^{11,9}, T. Inagaki¹¹, I. Kato¹¹, T. Nakaya¹¹, K. Nishikawa¹¹, T.J. Haines^{12,4}, S. Dazeley¹³, S. Hatakeyama¹³, R. Svoboda¹³, E. Blaufuss¹⁴, M.L. Chen¹⁴, J.A. Goodman¹⁴, G. Guillian¹⁴, G.W. Sullivan¹⁴, D. Turcan¹⁴, K. Scholberg¹⁵, A. Habig¹⁶, M. Ackermann¹⁷, J. Hill¹⁷, C.K. Jung¹⁷, K. Martens^{17,§}, C. Mauger¹⁷, C. McGrew¹⁷, E. Sharkey¹⁷, B. Viren^{17,3}, C. Yanagisawa¹⁷, T. Toshito¹⁸, C. Mitsuda¹⁹, K. Miyano¹⁹, T. Shibata¹⁹, Y. Kajiyama²⁰, Y. Nagashima²⁰, K. Nitta²⁰, M. Takita²⁰, H.I. Kim²¹, S.B. Kim²¹, J. Yoo²¹, H. Okazawa²², T. Ishizuka²³, M. Etoh²⁴, Y. Gando²⁴, T. Hasegawa²⁴, K. Inoue²⁴, K. Ishihara²⁴, J. Shirai²⁴, A. Suzuki²⁴, M. Koshihara²⁵, Y. Hatakeyama²⁶, Y. Ichikawa²⁶, M. Koike²⁶, K. Nishijima²⁶, H. Ishino²⁷, R. Nishimura²⁷, Y. Watanabe²⁷, D. Kielczewska^{28,4,¶}, H.G. Berns²⁹, S.C. Boyd²⁹, A.L. Stachyra²⁹, R.J. Wilkes²⁹

¹ Institute for Cosmic Ray Research, University of Tokyo, Kashiwa, Chiba 277-8582, Japan

² Department of Physics, Boston University, Boston, MA 02215, USA

³ Physics Department, Brookhaven National Laboratory, Upton, NY 11973, USA

⁴ Department of Physics and Astronomy, University of California, Irvine, Irvine, CA 92697-4575, USA

⁵ Department of Physics, California State University, Dominguez Hills, Carson, CA 90747, USA

⁶ Department of Physics, George Mason University, Fairfax, VA 22030, USA

⁷ Department of Physics, Gifu University, Gifu, Gifu 501-1193, Japan

⁸ Department of Physics and Astronomy, University of Hawaii, Honolulu, HI 96822, USA

⁹ Institute of Particle and Nuclear Studies, High Energy Accelerator Research Organization (KEK), Tsukuba, Ibaraki 305-0801, Japan

¹⁰ Department of Physics, Kobe University, Kobe, Hyogo 657-8501, Japan

¹¹ Department of Physics, Kyoto University, Kyoto 606-8502, Japan

¹² Physics Division, P-23, Los Alamos National Laboratory, Los Alamos, NM 87544, USA

¹³ Department of Physics and Astronomy, Louisiana State University, Baton Rouge, LA 70803, USA

¹⁴ Department of Physics, University of Maryland, College Park, MD 20742, USA

¹⁵ Department of Physics, Massachusetts Institute of Technology, Cambridge, MA 02139, USA

¹⁶ Department of Physics, University of Minnesota, Duluth, MN 55812-2496, USA

¹⁷ Department of Physics and Astronomy, State University of New York, Stony Brook, NY 11794-3800, USA

¹⁸ Department of Physics, Nagoya University, Nagoya, Aichi 464-8602, Japan

¹⁹ Department of Physics, Niigata University, Niigata, Niigata 950-2181, Japan

²⁰ Department of Physics, Osaka University, Toyonaka, Osaka 560-0043, Japan

²¹ Department of Physics, Seoul National University, Seoul 151-742, Korea

²² International and Cultural Studies, Shizuoka Seika College, Yaizu, Shizuoka, 425-8611, Japan

²³ Department of Systems Engineering, Shizuoka University, Hamamatsu, Shizuoka 432-8561, Japan

²⁴ Research Center for Neutrino Science, Tohoku University, Sendai, Miyagi 980-8578, Japan

²⁵ The University of Tokyo, Tokyo 113-0033, Japan

²⁶ Department of Physics, Tokai University, Hiratsuka, Kanagawa 259-1292, Japan

²⁷ Department of Physics, Tokyo Institute of Technology, Meguro, Tokyo 152-8551, Japan

²⁸ Institute of Experimental Physics, Warsaw University, 00-681 Warsaw, Poland

²⁹ Department of Physics, University of Washington, Seattle, WA 98195-1560, USA

A search for the relic neutrinos from all past core-collapse supernovae was conducted using 1496 days of data from the Super-Kamiokande detector. This analysis looked for electron-type anti-neutrinos that had produced a positron with an energy greater than 18 MeV. In the absence of a signal, 90% C.L. upper limits on the total flux were set for several theoretical models; these limits ranged from 20 to 130 $\bar{\nu}_e \text{ cm}^{-2} \text{ s}^{-1}$. Additionally, an upper bound of 1.2 $\bar{\nu}_e \text{ cm}^{-2} \text{ s}^{-1}$ was set for the supernova relic neutrino flux in the energy region $E_\nu > 19.3 \text{ MeV}$.

PACS numbers: 95.85.Ry, 97.60.Bw, 14.60.Lm, 96.40.Tv

During a core-collapse supernova, approximately 10^{53} ergs of energy are released, about 99% of which are in the

form of neutrinos. To date, the only time that a burst of such neutrinos has been detected was in the case of SN1987A [1, 2]. However, it is generally believed that core-collapse supernovae have occurred throughout the universe since the formation of stars. Thus, there should exist a diffuse background of neutrinos originating from all the supernovae that have ever occurred. Detection of these supernova relic neutrinos (SRN) would offer insight about the history of star formation and supernovae explosions in the universe.

All types of neutrinos and anti-neutrinos are emitted in a core-collapse supernova, but not all are equally detectable. The $\bar{\nu}_e$ is most likely to be detected by Super-Kamiokande (SK), as it interacts primarily through inverse β decay ($\bar{\nu}_e p \rightarrow n e^+$, $E_e = E_\nu - 1.3$ MeV), which has a cross section that is two orders of magnitude greater than that of neutrino-electron elastic scattering. Hence, all discussion herein of the SRN spectrum refers only to the spectrum of $\bar{\nu}_e$.

Several methods have been used to model the SRN flux and spectrum [3, 4, 5, 6, 7, 8], with flux predictions ranging from $2 - 54 \text{ cm}^{-2} \text{ s}^{-1}$. In this paper, SK search results are compared to SRN predictions based on a galaxy evolution model [4], a cosmic gas infall model [5], cosmic chemical evolution studies [6], and observations of heavy metal abundances [7]. A model that assumes a constant supernova rate [4] was also considered; this model was used to set the previous SRN flux limit at Kamiokande-II [9].

It has been shown that neutrinos undergo flavor oscillation [10, 11, 12]. Therefore, an SRN spectrum that includes the effects of neutrino mixing was also considered. All six species of neutrinos are emitted during a core-collapse supernova. However, the $\bar{\nu}_\mu$ and the $\bar{\nu}_\tau$ decouple from the neutrinosphere earlier than the $\bar{\nu}_e$, resulting in a higher temperature for these flavors; thus, neutrino mixing would harden the $\bar{\nu}_e$ energy spectrum. The cross section for inverse β decay increases as the square of the $\bar{\nu}_e$ energy, so oscillation would enhance the SRN signal.

In the oscillation model [8], it is assumed that anti-neutrinos are not subjected to matter effects within the supernova and so the mixing is treated as vacuum oscillation. In general, matter effects may distort the energy spectrum as the anti-neutrinos propagate through the supernova. It has been argued [13, 14] that the $\bar{\nu}_e$ emerge from the supernova in a pure mass eigenstate and do not experience vacuum oscillation. However, the $\bar{\nu}_e$ flux at the Earth obtained by this calculation coincides with the flux described in the previous reference [8] if minor corrections are made. Since the mixing is modeled with vacuum oscillation, the small mixing angle MSW solutions have almost no effect on the SRN spectrum. In this analysis, only a large mixing angle MSW solution (LMA) was used to distort the SRN spectrum – the LMA solution is also favored by the available solar neutrino data [15, 16].

This paper presents the results of a search for SRNs in the Super-Kamiokande detector. SK is a water

Cherenkov detector, with a fiducial mass of 22.5 kton, located in the Kamioka Mine in Gifu, Japan. Descriptions of the detector can be found elsewhere [17, 18, 19]. The data reported here were collected between May 31, 1996, and July 15, 2001, yielding a total SRN search livetime of 1496 days. Backgrounds to the SRN signal are solar neutrinos, atmospheric neutrinos, and muon-induced spallation products. Background reduction takes place in the following steps: first reduction, spallation cut, sub-event cut, Cherenkov angle cut, and solar neutrino cut.

The first reduction includes selection criteria to remove events that were induced by electronic noise, events that originated outside of the fiducial volume, and events that were reconstructed poorly. Additionally, decay electrons from stopping muons are removed at this stage by eliminating all events that occur within 50 microseconds after the previous event.

Spallation is the most serious background, and the ability to remove it from the data is the determining factor in setting the lower threshold of the SRN search. High energy cosmic ray muons induce spallation in oxygen nuclei within the detector. The resulting nuclei are unstable and undergo radioactive decay, emitting electrons with energies ranging from $\sim 3 - 20.8$ MeV. Due to the energy resolution of SK, there is a small possibility that spallation products will be reconstructed with energies as high as ~ 30 MeV. Thus, the spallation cut is applied to all events reconstructed with $E < 34$ MeV.

The spallation background is also relevant to solar neutrino studies, and so a likelihood function had been developed that uses information about the muons preceding the possible spallation event [11]. In order to permit a low analysis threshold for the SRN search, a tighter spallation cut was implemented. Therefore, in addition to the standard likelihood function cut, all events that occur less than 0.15 seconds after a cosmic ray muon are rejected. The strong timing cut was designed to exploit the fact that the highest energy spallation products are produced by the unstable nuclei with the shortest half-lives. The full spallation cut introduces an effective detector deadtime of 36%. No discernible spallation events with energies above 18 MeV remain in the data after this cut is applied and so 18 MeV was set as the lower analysis threshold.

The sub-event cut was implemented to remove muons with kinetic energy (T) in the range of 50–140 MeV. Cosmic ray muons, which have much higher energies, originate outside of SK and are removed from the sample during the first reduction because they produce a veto signal in the SK outer detector (OD). However, atmospheric ν_μ can produce muons at these low energies within the inner detector (ID) via charged current quasi-elastic scattering ($\nu_\mu N \rightarrow \mu N'$); such muons will not have been tagged by the OD, but will be visible in the ID. Due to their low energy, these muons will stop in SK and produce a decay electron; often the muon and its decay electron are found in the same event. When this happens, the decay electron is referred to as a “sub-event.” After the ver-

TABLE I: Number of events remaining after each reduction step. The energy of these events ranges from 18 MeV to 82 MeV.

Analysis step	Number of events
First reduction	1,602
Spallation cut ($E < 34$ MeV)	992
Sub-event cut	828
Cherenkov angle cut	278
Solar direction cut ($E < 34$ MeV)	271
Total events	271

tex of each event was found and the flight time of the Cherenkov photons was subtracted, the event's 1.3 microsecond timing window was searched; if more than one timing peak was present, then the event was removed. The sub-event cut was tested on simulated muons in the relevant energy range, and it was found to remove 34% of the muon background.

The remainder of the muons are removed by the Cherenkov angle cut. This cut exploits the mass difference between the muon and the positron, which results in a difference in their Cherenkov angles. The Cherenkov angle θ_C is determined by $\cos(\theta_C) = (n \times \beta)^{-1}$. In water, the index of refraction n is about 1.34. Positrons with $E > 18$ MeV will have $\beta \approx 1$, and thus $\theta_C \approx 42$ degrees. Muons with $T < 140$ MeV will have $\beta < 0.90$ and $\theta_C < 34$ degrees; therefore, all particles with $\theta_C < 37$ degrees were removed from the data. The efficiency of this selection criterion for retaining signal is 98%, as determined by applying it to simulated positron events. Using simulated muon events, it was also shown that the application of both the Cherenkov angle cut and the sub-event cut results in the rejection of 96% of the muon background. Furthermore, it was found that the full reduction resulted in the removal of $> 99\%$ of the muons. The Cherenkov angle cut was also used to remove events where the reconstructed angle was > 50 degrees; this eliminated events without clear Cherenkov rings from the data sample, such as multiple γ rays emitted during a nuclear de-excitation.

Finally, a cut on the direction of the event is made to remove possible contamination from solar neutrinos. The 18 MeV analysis threshold is low enough to permit some *hep* solar neutrinos to enter the sample. Additionally, ^8B solar neutrinos could also enter the SRN sample due to the energy resolution of SK. Thus, all events with $E < 34$ MeV and $\cos(\theta_{\text{sun}}) > 0.866$ were removed, where θ_{sun} is the angular separation between the reconstructed direction of the event and the vector that connects the Sun and the Earth at the time of the event.

By simulating positrons created from SRN, it was found that the combined efficiency of the data reduction is $47 \pm 0.4\%$ for $E \leq 34$ MeV, and $79 \pm 0.5\%$ for

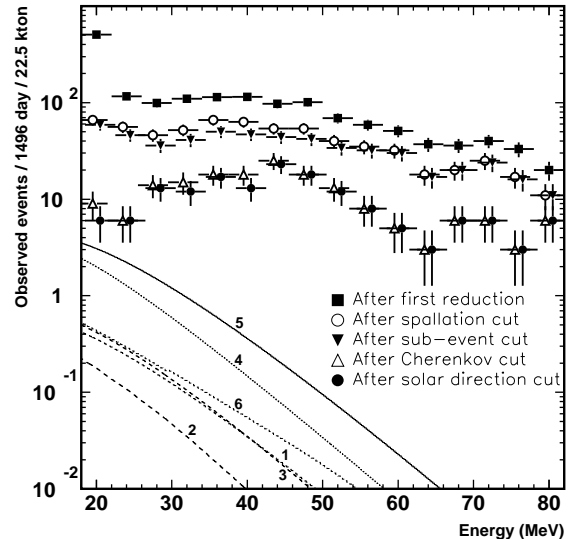


FIG. 1: Energy spectrum at each reduction step. In the final data set, the spallation cut and solar direction cut are only applied in the first four bins. The numbered lines represent the corresponding theoretical predictions from Table II.

$E > 34$ MeV. Table I summarizes the steps in the data reduction and notes how many events are left after each cut; Figure 1 plots the spectrum after each cut.

Even after applying the cuts described above, two sources of irreducible background remain. The first source is atmospheric ν_e and $\bar{\nu}_e$ events. The second source comes from atmospheric ν_μ that interact to form a muon that has $T < 50$ MeV. The total energy of these muons is below the threshold for emitting Cherenkov photons and so these muons are said to be invisible. Decay electrons from visible muons are removed in the first reduction; however, when an invisible muon decays there is no way to tag the resulting electron as a background event.

The energy spectra of the two irreducible backgrounds have shapes that are very different from each other and also from the shape of the predicted SRN signal. In the region where SRN events are expected (18 – 34 MeV), the dominant background source is decay electrons from invisible muons, which have energies that are distributed according to the Michel spectrum. However, at higher energies, contributions from atmospheric ν_e events distort the Michel spectrum. Thus, in order to perform a reliable fit to the decay electron background, it is necessary to extend the upper analysis threshold to the region where only atmospheric ν_e are present so that this distortion may be evaluated. Decay electrons have a maximum energy of 53 MeV. Energy resolution in SK smears this spectrum so that decay electrons can be detected up to ~ 65 MeV, above which only atmospheric ν_e are found. The upper analysis threshold was set in the energy region

that contains only atmospheric ν_e and the reduced data was analyzed with a three parameter fit.

To determine the final shape of the backgrounds, 100 years of simulated events were generated per background. The initial shape of the decay electrons was determined by the Michel spectrum; the initial shape of the atmospheric ν_e events was obtained from previous works [20, 21]. The background simulations were subjected to the full reduction, and the shape of the resulting spectra were used to fit the data; each of the SRN models was treated similarly. For the fitting, the data was divided into sixteen energy bins, each 4 MeV wide (see Figure 2), and the following χ^2 function was minimized with respect to α , β , and γ .

$$\chi^2 = \sum_{l=1}^{16} \frac{[(\alpha \cdot A_l) + (\beta \cdot B_l) + (\gamma \cdot C_l) - N_l]^2}{\sigma_{data}^2 + \sigma_{sys}^2} \quad (1)$$

In this equation, the sum l is over all energy bins and N_l is the number of events in the l^{th} bin. A_l , B_l , and C_l represent, respectively, the fractions of the SRN spectrum, the Michel spectrum, and the atmospheric ν_e spectrum that are expected to be in the l^{th} bin. α , β , and γ are the fitting parameters for the number of SRN events, decay electrons, and atmospheric ν_e events.

The total number of data events in the SRN candidate sample is small, and so the statistical error of the data σ_{data} is the dominant term in the denominator. The systematic error parameter σ_{sys} considers the effects that uncertainties in the spectrum shapes have on the SRN result. Such uncertainties originate from the reduction, the SK energy resolution, the theoretical atmospheric ν_e spectrum, and other sources. In all bins, the systematic error is approximately 6%, which is always much smaller than the statistical error.

Figure 2 shows the efficiency-corrected event rate spectrum of SRN candidates, as well as the result of the fit. The best fit to γ is indicated by the dot-dashed line and the best fit to β is indicated by the dotted line. The solid line is the sum of these two lines, which represents the total number of background events. For all six models, the best fit to α was zero. The minimum χ^2 value was found to be 8.1 for 13 degrees of freedom. In the absence of a signal, a 90% C.L. limit on α was found for each theoretical model. The dashed line in Figure 2 represents the sum of the background and the upper bound on α for the galaxy evolution model. This line details the type of distortion in the decay electron shape that would be indicative of an SRN signal.

From Figure 2, it can be seen that the expected backgrounds fit the data well. In this analysis, no overall flux normalization was chosen for the absolute rate of these background sources; only the shape was used. This is because there exists a large degree of uncertainty ($\sim 30\%$) in the atmospheric neutrino fluxes at these very low energies. However, a consistency check can be done by comparing the fit results for the total number of background events to the predictions. The predictions were

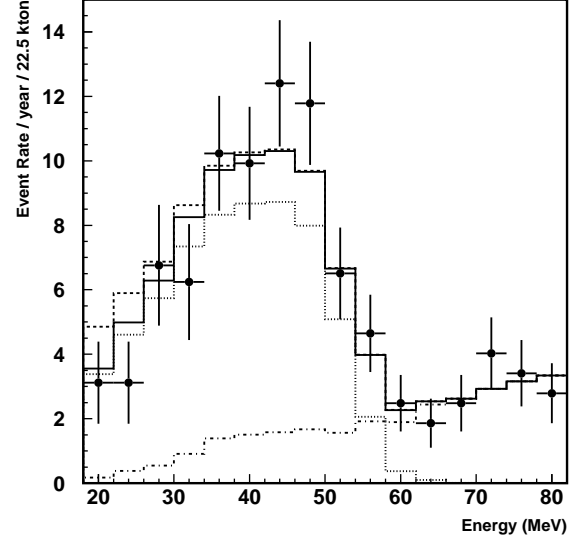


FIG. 2: Energy spectrum for SRN candidates in SK-I. The dotted and dash-dot histograms are the fitted backgrounds from invisible muons and atmospheric ν_e , respectively. The solid histogram is the sum of these two backgrounds. The dashed line shows the sum of the total background and the 90% upper limit of the SRN signal.

determined by taking 100 years of simulated background events, applying the reduction cuts, and normalizing for livetime. For the full 1496 days of SK livetime, the expected number of atmospheric ν_e events is 75 ± 23 , which is consistent with the best fit result of 88 ± 12 events. To determine the expected number of decay electrons created from invisible muons, neutrino oscillation must be considered [10]; given the low energy of the atmospheric ν_μ that produce invisible muons, it is assumed that half of these ν_μ have oscillated into ν_τ . With this assumption, the predicted number of decay electron events is 145 ± 43 , which is again consistent with the best fit result of 174 ± 16 events.

The limit on the value of α can be used to derive a 90% C.L. limit on the SRN flux from each theoretical model. The predicted number of SRN events is related to the flux by the following equation:

$$\alpha = N_p \times \tau \int_{19.3 \text{ MeV}}^{\infty} F(E_\nu) \sigma(E_\nu) \epsilon(E_\nu) dE_\nu \quad (2)$$

In this equation, N_p is the number of free protons in SK (1.5×10^{33}), τ is the detector livetime (1496 days, or $\sim 1.29 \times 10^8$ seconds), $\epsilon(E)$ is the signal detection efficiency, $\sigma(E)$ is the cross section for the inverse β decay ($9.52 \times 10^{-44} \text{ E}_e \text{ p}_e$), and $F(E)$ is the theoretical flux. The integral runs over the energy range of the neutrinos that produce positrons in the directly observed region.

By rewriting the flux as $F(E) = F \times f(E)$, where $f(E)$ is the normalized spectrum shape of the SRN flux and F

TABLE II: The SRN search results are presented for six theoretical models. The first column describes the method used to calculate the SRN flux. The second column shows the efficiency-corrected limit on the SRN event rate at SK. The third column is the flux limit set by SK, which can be compared with the theoretical predictions that are shown in the fourth column. The fifth column shows the flux predictions above a threshold of $E_\nu > 19.3$ MeV. Note that the heavy metal abundance calculation only sets a theoretical upper bound on the SRN flux [7].

Theoretical model	Event rate limit (90% C.L.)	SRN flux limit (90% C.L.)	Predicted flux	Predicted flux ($E_\nu > 19.3$ MeV)
Galaxy evolution [4]	< 3.2 events / year	$< 130 \bar{\nu}_e \text{ cm}^{-2} \text{ s}^{-1}$	$44 \bar{\nu}_e \text{ cm}^{-2} \text{ s}^{-1}$	$0.41 \bar{\nu}_e \text{ cm}^{-2} \text{ s}^{-1}$
Cosmic gas infall [5]	< 2.8 events / year	$< 32 \bar{\nu}_e \text{ cm}^{-2} \text{ s}^{-1}$	$5.4 \bar{\nu}_e \text{ cm}^{-2} \text{ s}^{-1}$	$0.20 \bar{\nu}_e \text{ cm}^{-2} \text{ s}^{-1}$
Cosmic chemical evolution [6]	< 3.3 events / year	$< 25 \bar{\nu}_e \text{ cm}^{-2} \text{ s}^{-1}$	$8.3 \bar{\nu}_e \text{ cm}^{-2} \text{ s}^{-1}$	$0.39 \bar{\nu}_e \text{ cm}^{-2} \text{ s}^{-1}$
Heavy metal abundance [7]	< 3.0 events / year	$< 29 \bar{\nu}_e \text{ cm}^{-2} \text{ s}^{-1}$	$< 54 \bar{\nu}_e \text{ cm}^{-2} \text{ s}^{-1}$	$< 2.2 \bar{\nu}_e \text{ cm}^{-2} \text{ s}^{-1}$
Constant supernova rate [4]	< 3.4 events / year	$< 20 \bar{\nu}_e \text{ cm}^{-2} \text{ s}^{-1}$	$52 \bar{\nu}_e \text{ cm}^{-2} \text{ s}^{-1}$	$3.1 \bar{\nu}_e \text{ cm}^{-2} \text{ s}^{-1}$
Large mixing angle osc. [8]	< 3.5 events / year	$< 31 \bar{\nu}_e \text{ cm}^{-2} \text{ s}^{-1}$	$11 \bar{\nu}_e \text{ cm}^{-2} \text{ s}^{-1}$	$0.43 \bar{\nu}_e \text{ cm}^{-2} \text{ s}^{-1}$

is the total flux of SRNs integrated over the entire spectrum, this equation can be inverted into the following:

$$F = \frac{\alpha}{N_p \times \tau \int_{19.3 \text{ MeV}}^{\infty} f(E_\nu) \sigma(E_\nu) \epsilon(E_\nu) dE_\nu} \quad (3)$$

Using the above values, the 90% C.L. SRN flux limit was calculated for each model. The results are in the third column of Table II, and can be compared with the predictions, which are in the fourth column. For the galaxy evolution model [4], the cosmic gas infall model [5], and the cosmic chemical evolution model [6], the SK limits are larger than the predictions by a factor of three to six. In these models, the dominant contribution to the SRN flux comes from supernovae in the early universe, so the neutrino energy is red-shifted below the 18 MeV threshold. The heavy metal abundance model primarily considers supernovae at red-shifts $z < 1$, so SK is sensitive to more of the SRN flux. For this model, the flux limit is smaller than the calculated total flux [7]. However, this prediction is only a theoretical upper limit, so these results can constrain this model but they cannot eliminate it. The LMA model [8] has a harder energy spectrum, and so SK is sensitive to a larger fraction of the SRN flux. The increased sensitivity is offset by the fact that this hardened spectrum also results in a larger limit for α ; thus, the SK flux limit is still nearly a factor of three larger than the prediction.

The total SRN flux predicted by the constant model can scale with the assumed rate of core-collapse supernovae. Thus, the SRN flux limit can be used to set a 90% C.L. upper limit on the constant supernova rate. The SRN flux prediction quoted in this paper is based on a reasonable supernova rate of $1.6 \times 10^3 \text{ SN year}^{-1} \text{ Mpc}^{-3}$. The observed SRN flux limit ($20 \bar{\nu}_e \text{ cm}^{-2} \text{ s}^{-1}$) corresponds to a supernova rate limit of $6.2 \times 10^2 \text{ SN year}^{-1} \text{ Mpc}^{-3}$. The constant model can therefore be ruled out, as this upper bound on the constant supernova rate is too low to be consistent with

the observed abundance of oxygen [4, 22], which is synthesized within the massive stars that eventually become supernovae. At Kamiokande-II, a flux limit of $780 \bar{\nu}_e \text{ cm}^{-2} \text{ s}^{-1}$ was set with the assumption of a constant supernova model [9]; the SK limit on this model is 39 times more stringent.

The SRN limits vary greatly, based on the shape of the theoretical SRN spectrum at energies that are below SK's SRN analysis threshold. To remove this strong model dependence, a limit was set for $E_\nu > 19.3$ MeV. In this region, all six models have similar energy spectrum shapes, and so an experimental limit that is insensitive to the choice of model can be obtained as follows:

$$F_{ins} = F \times \frac{\int_{19.3 \text{ MeV}}^{\infty} f(E_\nu) dE_\nu}{\int_0^{\infty} f(E_\nu) dE_\nu} \quad (4)$$

Flux limits in this energy region were the same for all models considered: $1.2 \bar{\nu}_e \text{ cm}^{-2} \text{ s}^{-1}$. Previously, the best limit of the SRN flux in this region was set using 357 days of data at Kamiokande-II [23]. This limit was $226 \bar{\nu}_e \text{ cm}^{-2} \text{ s}^{-1}$; the current SK limit is two orders of magnitude lower.

In summary, a search was conducted at Super-Kamiokande to detect the diffuse signal of $\bar{\nu}_e$ from all previous core-collapse supernovae. No appreciable signal was detected in 1496 days of SK data. Based on various theoretical models, 90% C.L. limits were set on the total SRN flux. A limit of $1.2 \bar{\nu}_e \text{ cm}^{-2} \text{ s}^{-1}$ was set for the SRN flux above the analysis threshold of $E_\nu > 19.3$ MeV. These results are more than an order of magnitude better than previous limits; some theories regarding the supernova rate in the universe can be constrained or rejected by these limits.

The authors gratefully acknowledge the cooperation of the Kamioka Mining and Smelting Company. The Super-Kamiokande detector has been built and operated from funds provided by the Japanese Ministry of Education,

Culture, Sports, Science, and Technology; the U.S. Department of Energy; and the U.S. National Science Foun-

dation.

-
- [*] Present address: Harvard University, Cambridge, MA 02138, USA
- [†] Present address: Enrico Fermi Institute, University of Chicago, Chicago, IL 60637, USA
- [‡] Present address: The Institute of Physical and Chemical Research (RIKEN), Wako, Saitama 351-0198, Japan
- [§] Present address: Department of Physics, University of Utah, Salt Lake City, UT 84112, USA
- [¶] Supported by Polish KBN grant 5P03B06531
- [1] K.S. Hirata *et al.*, Phys. Rev. D **38**, 448 (1988); K.S. Hirata *et al.*, Phys. Rev. Lett. **58**, 1490 (1987).
- [2] C.B. Bratton *et al.*, Phys. Rev. D **37**, 3361 (1988); R.M. Bionta *et al.*, Phys. Rev. Lett. **58**, 1494 (1987).
- [3] T. Totani and K. Sato, Astropart. Phys. **3**, 367 (1995).
- [4] T. Totani, K. Sato, and Y. Yoshii, Astrophys. J. **460**, 303 (1996). The cosmological parameters of the model used in this paper are $(h, \Omega, \lambda) = (0.8, 0.2, 0.8)$.
- [5] R. A. Malaney, Astropart. Phys. **7**, 125 (1997).
- [6] D. H. Hartmann and S. E. Woosley, Astropart. Phys. **7**, 137 (1997). The “NC” model is used here, which was selected by the authors as their standard model.
- [7] M. Kaplinghat, G. Steigman, and T. P. Walker, Phys. Rev. D **62**, 043001 (2000).
- [8] S. Ando, K. Sato, and T. Totani, Astropart. Phys. (to be published). The supernova model used here is “SN1,” and the mixing is described by “LMA-L.”
- [9] K. S. Hirata, PhD thesis, University of Tokyo (1991).
- [10] Y. Fukuda *et al.*, Phys. Rev. Lett. **81**, 1562 (1998).
- [11] S. Fukuda *et al.*, Phys. Rev. Lett. **86**, 5651 (2001).
- [12] Q. R. Ahmad *et al.*, Phys. Rev. Lett. **87**, 071301 (2001).
- [13] A. Y. Smirnov, D. N. Spergel, and J. N. Bahcall, Phys. Rev. D **49**, 1389 (1994).
- [14] A. S. Dighe and A. Y. Smirnov, Phys. Rev. D **62**, 033007 (2000).
- [15] S. Fukuda *et al.*, Phys. Lett. B **539**, 179 (2002).
- [16] Q. R. Ahmad *et al.*, Phys. Rev. Lett. **89**, 011302 (2002).
- [17] M. Nakahata *et al.*, Nucl. Instrum. Methods Phys. Res. Sect. A **421**, 113 (1999).
- [18] Y. Fukuda *et al.*, Phys. Rev. Lett. **82**, 2430 (1999).
- [19] Y. Fukuda *et al.*, Phys. Rev. Lett. **82**, 1810 (1999).
- [20] Y. Fukuda *et al.*, Phys. Lett. B **433**, 9 (1998).
- [21] G. Barr, T. K. Gaisser, and T. Stanev, Phys. Rev. D **39**, 3532 (1989).
- [22] W. D. Arnett, D. N. Schramm, and J. W. Truran, Astrophys. J. **339**, L25 (1989).
- [23] W. Zhang *et al.*, Phys. Rev. Lett. **61**, 385 (1988)